PelVis: Atlas-based Surgical Planning for Oncological Pelvic Surgery

Noeska Smit, Kai Lawonn, Annelot Kraima, Marco DeRuiter, Hessam Sokooti,
Stefan Bruckner, Elmar Eisemann, and Anna Vilanova

Abstract—Due to the intricate relationship between the pelvic organs and vital structures, such as vessels and nerves, pelvic anatomy is often considered to be complex to comprehend. In oncological pelvic surgery, a trade-off has to be made between complete tumor resection and preserving function by preventing damage to the nerves. Damage to the autonomic nerves causes undesirable post-operative side-effects such as fecal and urinal incontinence, as well as sexual dysfunction in up to 80 percent of the cases. Since these autonomic nerves are not visible in pre-operative MRI scans or during surgery, avoiding nerve damage during such a surgical procedure becomes challenging. In this work, we present visualization methods to represent context, target, and risk structures for surgical planning. We employ distance-based and occlusion management techniques in an atlas-based surgical planning tool for oncological pelvic surgery. Patient-specific pre-operative MRI scans are registered to an atlas model that includes nerve information. Through several interactive linked views, the spatial relationships and distances between the organs, tumor and risk zones are visualized to improve understanding, while avoiding occlusion. In this way, the surgeon can examine surgically relevant structures and plan the procedure before going into the operating theater, thus raising awareness of the autonomic nerve zone regions and potentially reducing post-operative complications. Furthermore, we present the results of a domain expert evaluation with surgical oncologists that demonstrates the advantages of our approach.

Index Terms—Atlas, surgical planning, medical visualization

◆

1 INTRODUCTION

Oncological surgical procedures in the pelvic area are often performed to treat rectal, cervical and prostatic cancer. Due to the funnel shape of the pelvic cavity, the pelvic organs are arranged in close proximity, surrounded by vital structures such as the arteries, nerves, and lymphatic system. For this reason, pelvic anatomy is often considered to be complex. In oncological pelvic surgery, a thorough understanding of the pelvic anatomy is crucial to the success of the procedure. While removal of the tumor and a tumor-free circumferential margin is the main priority, the pelvic autonomic nerves should not be damaged in order to preserve function post-operatively. Due to damage to the autonomic nerves during a total mesorectal excision, this procedure results in urinal incontinence in 33.7% of the cases, fecal incontinence in 38.8%, and sexual dysfunction in up to 80% of the patients [24, 47]. Unfortunately, due to the limited size of the autonomic nerves, they are not visible in pre-operative Magnetic Resonance Imaging (MRI) scans or during surgery. Therefore, surgeons must rely on their anatomical knowledge to avoid damage to the autonomic nerves. Until recently, there was no anatomical consensus on the exact relation of these autonomic nerves to the fascia sheets, further complicating a uniform choice of surgical dissection planes [19].

Recently, the Virtual Surgical Pelvis (VSP), an atlas model of the female pelvis, has been developed, which contains all surgically relevant structures in the female pelvis. In this atlas model, surgical risk zones

• Noeska Smit is with the Delft University of Technology, and the University of Bergen. E-mail: noeska.smit@uib.no.
• Kai Lawonn is with the University of Koblenz · Landau. E-mail: lawonn@uni-koblenz.de.
• Anne C. Kraima, Marco DeRuiter, and Hessam Sokooti are with the Leiden University Medical Center. E-mail: a.c.kraima@lumc.nl, m.c.de_ruiter@lumc.nl, and h.sokooti_oskooyi@lumc.nl
• Stefan Bruckner is wih the University of Bergen. E-mail: stefan.bruckner@uib.no.
• Elmar Eisemann and Anna Vilanova are with the Delft University of Technology. E-mail: e.eisemann@tudelft.nl, and a.vilanova@tudelft.nl.

in which the autonomic nerves reside are indicated. By registering this atlas to patient-specific MRI scans, we are able to visualize the autonomic nerve zones in the context of an individual patient. After the registration process, we can construct a patient-specific 3D model of the surgically relevant structures that can be used in surgical planning and education for oncological surgeons in order to increase awareness of the regions at risk for nerve damage. Due to the anatomical complexity of the pelvis, many structures occlude a clear view on the structure that is to be resected, while they are still necessary as anatomical context. Furthermore, the proximity of the autonomic nerves to the target organ, as well as the distance of the tumor to the organ border are important aspects in planning the procedure. In our approach, we present several visualization methods to visualize target, risk and context structures for surgical planning. For this, we employ occlusion-management and distance-based visualizations to satisfy the surgical planning requirements. We demonstrate the utility of these methods in an interactive application designed for surgical planning of the total mesorectal excision procedure. In several linked 2D and 3D views, the surgeon is able to explore the spatial relations and distances between surgically relevant structures based on MRI and registered atlas information.

With this, our contributions are the following: (1) We present visualization methods tailored to evaluate distances and to avoid occlusion in surgical-planning visualizations for oncologic procedures. (2) We provide an interactive application based on these methods for surgical planning of the total mesorectal excision procedure. (3) We present an evaluation with five domain experts and ten non-experts in which we demonstrate the utility of our approach.

2 RELATED WORK

In this section, we describe work related to our method, such as visualization methods for surgical planning and general visualization techniques applicable in our context.

Much work has been done on applying visualization techniques to improve surgical planning, mainly in orthopedic, hepatic, facial and neurosurgery. A full overview of these surgical planning methods is out of the scope of this paper, but additional information can be found in the book by Preim and Botha [37].

Estimating distances between organs and relevant structures is an important task during surgical planning. Some previous works in surgical planning have used color mapping and isolines to encode distances.

Marai et al. proposed a method for estimating joint contact areas in which they combine a colormap with isolines to visualize distances on the bone surfaces [27]. Dick et al. presented several methods for distance visualization in interactive 3D orthopedic implant planning [7]. They propose two methods to visualize the distance of the implant to the bone besides color mapping: slice-based distance visualization and glyph-based distance visualization. Both methods only visualize a single anatomical structure. Süßmuth et al. presented a color-encoded distance visualization of cranial nerve-vessel contacts for diagnosis and treatment of neurovascular compression (NVC) syndromes [43]. They employ a slice-based colored isoline visualization and also color-code the distances in 3D surface models. While the vessels were semi-automatically segmented, the nerves were added by manual segmentation. Rieder et al. presented a method where color and isolines were used to encode heat distribution successfully in radiofrequency ablation [39]. Using their GPU-based heat distribution calculation method, they visualize heating and cooling zones in 2D slices as well as 3D volume rendering. Since we have numerous structures to visualize and due to the complex pelvic anatomy, we employ isolines and color-coding on the resection target surface only in order to prevent further visual overload and clutter.

Regarding the visualization of distances to aid risk assessment, Hansen et al. employ discrete color coding to visualize robust safety margins for oncologic liver surgery [14]. Based on a distance calculation, they visualize which vascular structures would be affected by choosing a certain safety margin around the tumor in the planned resection. Besides the target and risk areas, no contextual anatomical structures are shown. Marshall et al. proposed a Proximity Map Projection (PMP) for interactive visualisation for surface proximity monitoring [28]. They apply their technique in the context of real-time MRI for the guidance of thermal therapy and show a mapping of the 3D distances to a 2D representation. Krüger et al. proposed an interactive visualization for oncological procedure planning in head and neck surgery [22]. They employ several visualization methods such as cutaway views, silhouettes and color-coded distances in an interactive surface-based application. Their work is the most closely related to ours, since it also involves complex anatomy and pathology with many structures in close spatial relations, though the excision goal is a tumor and not a complete organ.

To improve the reliability of our visualizations, we visualize an estimation of the uncertainty due to the registration. Djurcilov et al. presented methods for visualizing uncertainty in volume rendering [8]. They employed holes, depth-shaded holes, noise and texture to visualize uncertainty together with scalar volumetric data. Grigoryan and Rheingans employed point-based primitives to show surface uncertainty [13]. Their approach displaces points on surfaces where they are uncertain, resulting in a fuzzy appearance. Since we need to preserve the shape and view on the organ, while visualizing registration confidence, our approach employs screenspace-oriented methods. Whitaker et al. presented contour boxplots to visualize uncertainty in simulation ensembles [49]. Our contour confidence visualization was inspired by their visualization, though we do not base it on an ensemble of contours. While not aimed at surgical planning, Termeer et al. encoded myocardial perfusion in a comprehensive visualization of the coronary anatomy [44]. The blood supply was shown using a combination of colormapping and isolines. In under-perfused regions, a striped pattern was blended in with faded edges to indicate uncertainty. This pattern approach inspired our grid and halftone confidence visualizations, though ours are generated in screen space.

To the best of our knowledge, there is no related literature on surgical planning for pelvic oncologic procedures. Compared to other surgical planning applications, our approach adds information that is not visible in the pre-operative medical scans by involving atlas information. Furthermore, we propose several visual encodings that communicate distance and confidence information simultaneously and evaluate these qualitatively with domain experts and quantitatively with non-experts.

3   MEDICAL BACKGROUND

The pelvic anatomy is often considered to be complex, due to the funnel shape, the organs and vital structures such as nerves, blood vessels and lymph nodes, are very closely related to each other. When surgery needs to be performed in the pelvis, this proximity of the structures, combined with limited access, complicate the procedure. Pelvic surgery often involves oncological procedures to treat cervical, prostatic and rectal cancer. Colorectal cancer is the second most common type of cancer in Europe and responsible for 215,000 deaths per year [9]. One third of colorectal cancer cases presents in the rectum.

In case of rectal malignancies, the gold standard surgical procedure is the total mesorectal excision (TME) [15]. Though other procedures exists to treat rectal cancer, the TME has lower recurrence rates [16]. In the TME, the rectum is resected, including removal of the mesorectum, a layer of fatty tissue surrounding the rectum. The anal sphincter can be spared and connected to the remaining bowel through anastomosis in the low anterior variant of the procedure. In case the tumor is situated too close to the anal sphincter (within 5 cm), an abdominoperineal resection (APR) needs to be performed, resulting in the removal of the anal sphincter and a permanent stoma.

The quality of a TME procedure is evaluated using several factors influencing the recurrence and survival rates. After the procedure, the circumferential resection margin (CRM), the distance of the resection border to the tumor, is checked by a pathologist [30]. The influence of the circumferential resection margin on local recurrence, distant metastasis and survival rates was studied by Wibe et al. [50]. They concluded that a decreasing circumferential margin is associated with an exponential increase in the local recurrence rates, metastasis and death. A margin of ≤ 1 mm is considered a negative prognostic factor for local recurrence [34]. Furthermore, the excised mesorectum specimen should be complete. If it is incomplete, there is an increased rate for local and distant recurrence [31].

While the recurrence and survival rates are crucial, preserving function is additionally an important factor in surgery. The TME procedure can result in urinal and fecal incontinence as well as sexual dysfunction if the autonomic nerves are damaged during the procedure.

The TME procedure can be performed in open surgery, in which the abdomen is cut open, or using a minimally invasive, or laparoscopic approach [26]. In laparoscopic surgery, also known as keyhole surgery, small incisions are made and the surgery is performed using a laparoscope, a flexible camera with a light source. Additionally, laparoscopic TME can also be performed aided by a robotic surgery [36]. While traditionally the TME procedure is executed in a cranio-caudal direction, there is a relatively new trend to approach the resection through the anus in the transanal minimally invasive surgery for total mesorectal excision (TAMISTME) [1].

Surgical planning for the TME procedure currently only consists of the analysis of a pre-operative MRI scan, which can be used to determine the type of surgery and in cancer staging [4,11]. The complex anatomy of the pelvic area makes it challenging for the surgeon to determine the exact anatomical relations between structures in 3D during the operation, given the MRI scans. Often anatomy textbooks are additionally also used to complement the MRI information.

4   REQUIREMENTS ANALYSIS

In order to elicit the requirements for our surgical planning tool, we consulted with two anatomists and two surgeons. From these discussions, we formulated a list of surgically relevant structures and derived features. The following structures are surgically relevant during the planning phase of a TME procedure: (1) the pelvic bones, (2) the vagina/uterus or prostate, (3) the bladder, (4) the mesorectum, (5) the tumor, and (6) the autonomic nerves.

The mesorectum is important since it is the structure that is to be resected during the TME procedure. The organs closely arranged around the mesorectum, i.e., the internal genitalia and bladder serve as spatial context and are recognizable during surgery. The pelvic bones also serve as spatial context and additionally feature anatomical landmarks that can be identified even externally, such as the spina iliaca anterior superior. The tumor and its relation to the mesorectum
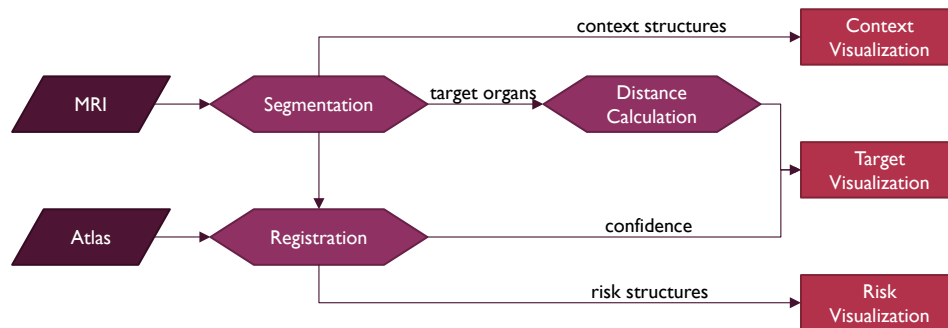
Fig. 1: The PelVis pipeline: With MRI and atlas input data, after three preprocessing steps, we visualize context, target and risk structures.

is important to determine the required type of surgery. The autonomic nerves are structures that need to be avoided during surgery, since damaging them negatively affects functional outcome.

Among these structures, a distinction can be made between structures that serve as an anatomical context to aid spatial orientation (structures 1 to 3), structures that need to be resected (structures 4 and 5) and structures that pose a risk for poor functional surgical outcome (structure 6). Therefore, we classify these structures conceptually into the following categories: context, target and risk structures.

Based on these structures, there are several derived features that influence the decision of what surgical procedure to perform and approach: tumor diameter, distance of the tumor to the anal sphincter, distance of the tumor to mesorectum border and distance of the mesorectum to the autonomic nerves. The tumor diameter and distance to the anal sphincter influence the staging and determine if an APR or low anterior resection have to be performed. The distance of the tumor to the mesorectal fascia influences if the circumferential resection margin is in danger of being positive, i.e., if tumor tissue is found in the resection border. The distance of the mesorectum to the autonomic nerves determines how careful surgeons need to be when cutting along that specific part of the mesorectum.

While the first three features are easily accessible from the MRI scan, the fourth feature is not, since the autonomic nerves are not visible in MRI scans. Our approach relies on registration to acquire these nerve zones and we must visualize the confidence in the registration success in order to not mislead the user. The MRI scan already provides much information, but for surgeons in training the translation between 2D MRI visualizations and 3D patient anatomy is more challenging.

It should be noted that, unlike for instance in biopsy planning or neurosurgery, in this procedure, there is no access path planning involved. The total mesorectum needs to be resected and there are no alternative approach paths among which the best must be selected. In our case we aim to increase awareness on the spatial extent of the patient-specific anatomy and pathology, as well as vital structures that are invisible both in MRI and during surgery and around which the surgeon has to be especially careful during the resection.

Based on this information, we formulated the following requirements in close collaboration with our domain experts:

- **Requirement 1:** The context and risk structures must be visualized in such a way that they do not occlude the target structures, while preserving shape perception.

- **Requirement 2:** The distance of the risk structures to the target structures and between the target structures must be perceivable from the visualization.

- **Requirement 3:** The relation between the MRI scan and 3D patient-specific models must be understandable from the visualization.

- **Requirement 4:** The user should be able to estimate the confidence in the result of the registration process.

By satisfying these four requirements our method aims to improve spatial understanding of anatomy and pathology, as well as risk assessment.

5 PELVIS

In this section, we describe our visualization design decisions with respect to the requirements and the components of our PelVis pipeline (Figure 1). Our method relies on MRI and atlas data as input and requires segmentation, registration and distance calculation as preprocessing steps (see Section 5.1). The resulting data and features are then used in three visualization methods aimed at visualizing context, target and risk structures (see Section 5.2). We discuss available interaction techniques in our application in Section 5.3.

5.1 Preprocessing

Since the risk structures, the regions where the autonomic nerves are located, are not visible in MRI scans, we make use of an atlas that contains these regions. To make the atlas patient-specific, we need to register the atlas labels to the MRI. Since our atlas is based on cryosectional data and does not feature MRI scans, the registration process is not straightforward. Existing registration methods are likely to fail since the information presented and resolution in both modalities is vastly different. The registration is further complicated because we are dealing with soft tissues that significantly vary in size and shape, depending on the patient or other factors, such as the bladder being filled or empty.

Most major structures, however, such as the target and context structures are visible in the MRI as well as the atlas. For our registration method, we make the assumption that the distance of the risk zones to the major organs is constant between patients. As discussed with our domain experts, while individual nerves and organ shapes vary, the zones in which they reside and the distances to the major organs do not. Based on this assumption, we can register the major organs in the atlas to the MRI and apply the same deformation field to the risk zones to map them to a patient-specific context.

To aid the registration process, we manually segment the major organs (bladder, vagina, mesorectum) and bones from the MRI. The result of this segmentation is used for two purposes. First, to aid the registration process by providing common structures available in both modalities. Additionally, this information is used to reconstruct patient-specific 3D models of target and context structures. More advanced techniques, which require less laborious manual work could be used for the segmentation. However, to test the concepts presented in this paper, we estimated that manual segmentation was the best option, since it does not introduce further inaccuracies that potentially arise from an automatic segmentation method.

The inputs to our registration step are the label volume containing the segmented structures from the MRI and the label volume of the matching structures in the atlas. In this case, the atlas labels represent our moving image data, while the MRI labels are our target image data. As an initialization, we perform a rigid alignment. After this, we want to deform the atlas structures locally to fit the MRI as closely as possible using an automatic deformable B-spline registration [40].

(a) Opaque   (b) Semi-transparent

(c) Ghosted   (d) Our approach
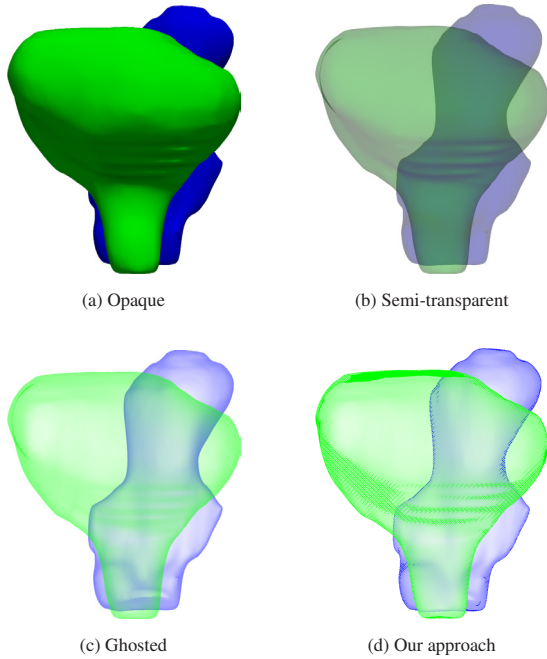
Fig. 2: Four different representations of two context structures: opaque, semi-transparent, ghosted view and our approach.

(a) Grid   (b) Halftone

(c) Isoline confidence   (d) Isoline blur

Fig. 3: Four combined confidence and distance visual encodings: a) blended gridlines, b) halftone, c) isoline confidence and d) isoline blur.

The specific implementation we used employs an adaptive stochastic gradient-descent optimization [20]. Due to the use of gradient information, registering label volumes directly is unlikely to be successful. Therefore, we calculate distance fields on both label volumes and use these as the input for the deformable registration step. The resulting deformation field is then applied to the risk structures from the atlas to map them into the patient-specific MRI. Due to the registration process, we might not be able to perfectly map all structures to each other, resulting in an uncertainty that we take into account in our visualization.

We rely on a simple indication of the registration success. Since we assume the proportional distance of the risk zones to the organs is preserved, we can estimate the registration success by checking how well the borders of the registered atlas organs align with the borders of the segmented MRI organs. To find this value, we check the distances for every point on the structure borders and scale them to a value between 0 and 1, where 0 indicates a perfect border alignment and 1 is a maximum difference. While more complex methods could be used to determine the confidence we have in the registration outcome, such as bootstrap resampling for uncertainty estimation [23], this is considered out of the scope of this paper.

Since visualization of the distances between the risk zones and target structures is a requirement (see Requirement 2), we calculate the distance between risk structures and target structures using an N-dimensional version of the Euclidian distance mapping proposed by Danielsson [6]. We calculate the distance field on the binary volumes containing the structures of interest. After the segmentation, registration and distance calculations are performed, we obtain the needed components that serve as the input to our visualization methods.

5.2 Visualization

Depending on the type of the structure, we have selected various visual encodings to support the user in relation to the requirements stated in the previous section. In this sub-section, we describe the design decisions made in visualizing the context, target and risk structures.

5.2.1 Context structures

The context structures serve to provide anatomical context during the surgical planning and are arranged in multiple layers. According to Requirement 1, we need to visualize them in such a way that they do
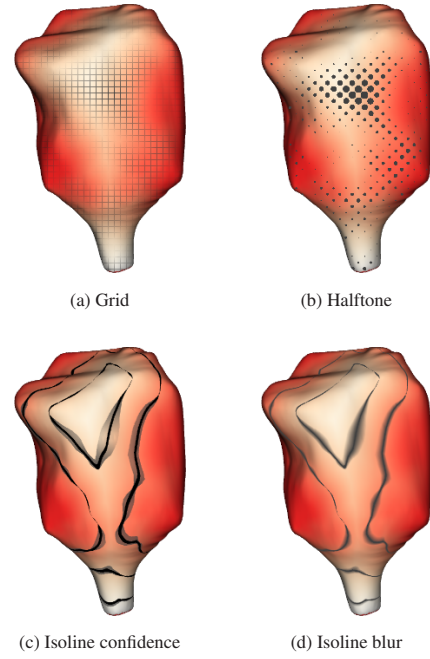
not obstruct the view on target structures, while maintaining their shape perception. This requirement rules out standard opaque rendering styles. Smart visibility techniques, which are illustrative and only convey the most important visual information via a high level of abstraction, can be used for occlusion management [46]. We combine two visualization techniques: a ghosted view to manage occlusion, and hatching to emphasize the shape and depth perception. The resulting visualization for the context organs is shown in Figure 2d.

While standard semi-transparent techniques could be employed, ghosted views have already shown to support an accurate spatial analysis of vessel structures with aneurysms [2]. In our application domain, we have several nested structures with complex shapes, for which semi-transparent approaches fail to provide enough shape and depth information (see Figure 2a and 2b). Therefore, to prevent occlusion of the target structures, we render the context structures as a ghosted view. In our ghosted view, we use a view-dependent transparency rendering that is more opaque at regions facing away and more transparent at regions facing towards the viewer (see Figure 2c). We use an approach similar to the one proposed by Gasteiger et al. in which the opacity is determined based on the Fresnel-reflection model [10].

Our ghosted view is able to prevent occlusion of the target structures, but makes shading perception more difficult than when using a standard semi-transparent representation. Both these rendering styles fail to convey the correct depth ordering. Therefore, we turn to illustrative techniques to emphasize the shape and depth ordering of the context structures. In the work by Interrante et al. [18], it was shown that the shape of a transparent surface and its relative depth distance from an underlying opaque object could be more accurately perceived when the surface is rendered with a sparse, opaque texture. Since we do not want to add to the pre-processing required for our method, we employ a simple hatching technique to convey shading and enhance the contour region perception. Hatching is able to provide shading cues without fully occluding the covered context structures or influencing the color perception of underlying structures. We chose to use image-based hatch strokes as developed by Lawonn et al. [25]. This hatching method is based on the dot product between the view direction and the surface normal and adds more strokes for 'darker' regions, where this dot product is small, when placing a light source at the camera position. To enhance the depth-ordering perception, we add a silhouette outline based on the same dot product (see Figure 2d). This approach

for rendering silhouette outlines is based on the method by Gooch et al. [12].

5.2.2 Target structures

The target structures are challenging to visualize in our application since they are nested; the tumor resides within the mesorectum. According to Requirement 2, we need to visualize both the distances of the risk structures to the targets, as well as the distances of the target structures among themselves, i.e., the tumor distance to the mesorectal wall. Furthermore, according to Requirement 4, we also need to visualize how confident we are in the calculated distances of the risk structures to the target structures, since they are the result of a registration process that introduces uncertainty.

After calculating the distance fields for both the risk structures and tumor in the preprocessing step, we visualize these by sampling the distances at the mesorectum border. For both distances, we employ a colormap from red to white to indicate proximity to the risk structures and the tumor respectively. We chose this colormap due to the intuitive meaning, i.e., red is dangerous and white is safe, and additionally because it does not interfere with the shading. To further enhance the distance perception, we add isolines at distances of interest. These isolines are formed by connection points of equal distance for several distances. Besides indicating these distances, these lines further emphasize the shape of the target structure, as contour lines such as these can enhance shaded surfaces to make a shape easier to perceive [48]. House and Ware state that contours can be thought of as a special type of texture that follows the shape of a surface [17]. In this way, we encode distances in a continuous representation using color mapping, as well as in a quantized manner using the isolines. While slice-based and glyph-based approaches worked well in the work by Dick et al. [7], the complex shape and spatial relationships of our target structures in relation to the risk zones, combined with the requirement to also visualize confidence, generates a situation in which clutter can become an issue. This makes a simple representation via color mapping and isolines a better visual encoding choice for our purposes.

Besides the distances, we also need to visualize the confidence that we have in the correctness of the risk-target distance calculation based on the registration success according to Requirement 4. For this, we calculate a local metric of registration confidence given by how well the registered structures of the atlas match up to the segmented MRI structures. We sample this metric at the mesorectal border and need to visualize the distance and the distance's confidence concurrently. While a separate view could be employed just to visualize confidence, our experts are only interested in the confidence and the distance simultaneously. A straightforward solution would be to map the confidence to color, but since we already encode distance using color, we looked into several alternatives that can be perceived simultaneously.

We developed two global visual encodings and two local visual encodings that are shown only near the isolines (see Figure 3). While textures could be employed to encode confidence [38], for our clinical context we do not want to perform texture-mapping beforehand and rely on screen-space solutions. For the first global option, we blend in a grid based on the amount of confidence. In regions where we are less confident, the grid is shown more clearly (see Figure 3a). The second option is to use a halftone pattern, where the size of the dots corresponds inversely to the confidence (see Figure 3b). In this case, large dots indicate that we are not confident about the distances in these areas. Both these options were selected in order not to interfere with the standard surface shading and hatching of the context structures.

Besides these two global representations, we also provide two localized visualization options. In the first, we show a 'confidence band' around the isolines (see Figure 3c). Here, a wider and lighter band indicates low confidence, while certain areas show a narrow dark band. In the second local option, we blur the isolines based on the amount of confidence (see Figure 3d). When confidence is low, the isolines are blended over a wider area than in areas where we are confident of the registration's success.
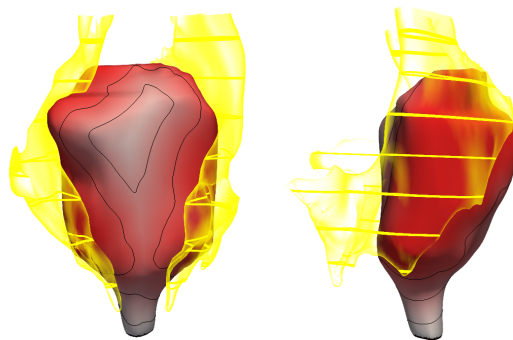
Fig. 4: Visualization of a target structure and risk structure from a frontal and side view.

5.2.3 Risk structures

The risk structures are similar to the context structures in that they should not occlude the target structures, according to Requirement 1. For this reason, we visualize them in a similar way by employing a ghosted view. The main difference in our application between the risk structures and the context structures, is that the risk zones are not an actual anatomical structure, but rather a zone in which the autonomic nerves are located. We do not employ hatching to differentiate the look of the risk zones from the other context organs. However, to emphasize height information, which is important for the surgical approach in relation to the height of the tumor, we add contour bands at fixed intervals. These contour bands also serve to emphasize the different shapes of the risk zones for varying heights (see Figure 4).

5.3 Interaction

To satisfy Requirement 3, we visualize the MRI data and patient-specific 3D models in linked views. Furthermore, we enrich the MRI with contours of the segmented and registered structures by placing colored lines on the intersection of the MRI plane and the 3D models. The colors of these lines correspond to the structure color in 3D to further enhance the link between the views.

The visualization of the target structures shows the mesorectum in an opaque way and since the tumor is nested within, it is not directly visible. To show the spatial relation between the tumor and the mesorectal fascia, we employ a cutting and unfolding interaction technique. This 'exploded view' was inspired by the volumetric brain cleaving by van Dixhoorn et al. [45], which is based on the Hinge Spreader technique proposed by McGuffin et al. [29]. Since the human body is mainly symmetric along a saggital plane, we place an interactive splitting plane that can be freely positioned in a region of interest. Then, the left and right halves of the structures can be interactively moved away from the center by rotation away from the center plane, similar to opening a book, combined with simultaneous translation (see Figure 6). The structures are rotated and translated subsequently in a staggered movement from outer to inner structures, which results in a interaction metaphor similar to peeling the model open layer by layer. In the center of the view, we place a copy of the uncut tumor for inspection along with the isolines that give an indication of the spatial extent of the mesorectum around the tumor. The unfolded visualization leaves space in the center for ghosted copies of individual structures to be shown when desired.

Based on the view during a surgical approach, we additionally define a default camera viewpoint from a similar perspective. In this 'surgical view', the pelvis is viewed from the top down, as is the case during both laparoscopic and open surgery. In this viewpoint, the unfolding movement is adjusted to take the current view into account.

6 IMPLEMENTATION

The required pre-processing MRI segmentation of the major organs was performed semi-automatically in AMIRA and MITK [51]. We used RegistrationShop [42] and Elastix [21] to perform the rigid and deformable B-spline registration respectively. After this, we reconstructed
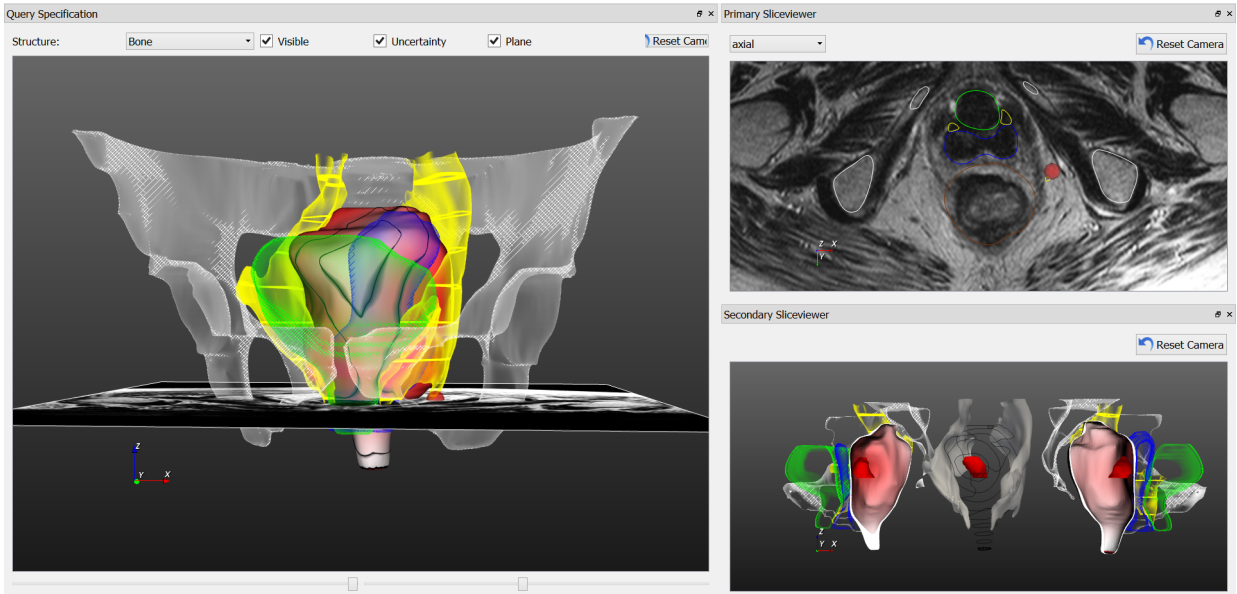
Fig. 5: The PelVis prototype application featuring the 3D model on the left and a linked MRI and unfolded view visualization on the right.

surfaces for the segmented organs and risk zones using DeVIDE [3]. Then, we calculated the distance fields from the nerve zones and tumor and stored this information in the mesorectum surface mesh. Finally, we calculated the distance confidence using a combination of DeVIDE and Matlab to compute the registration alignment mismatch from the organs, and also stored these values in the mesorectum mesh. To get the distance confidence, we employ a simple method, where we calculate a distance field over all organ edges, and sample this at the mesorectal border and normalize it, leaving us with an indication of the registration organ alignment success.

We implemented the visualization and interaction methods in a prototype application in Python using the Visualization Toolkit (VTK) and Qt for the interface, extended with custom GLSL vertex and fragment shaders, with separate shaders for context, risk and target structures. The target structure shaders employed the values stored in the mesorectum mesh to generate the target structure distance and confidence visualization. For the MRI contours, we simply cut the structure surfaces at the location of the MRI plane. For the unfolding, we cut the surface data into a left and right half at the user-specific plane location, and rotate and translate the halves in opposite directions.

7 RESULTS

For our prototype application, we used the VSP atlas which is based on the Visible Korean female cryosectional dataset [32, 33, 35]. We registered the atlas to five patient-specific pre-operative MRI scans of patients undergoing a TME procedure with various tumor locations and types and reconstructed the major surgically relevant structures and risk zones in 3D using our method.

A screenshot of the interface can be seen in Figure 5. In the 3D model the context structures are visualized in white (bone), green (bladder), and blue (vagina). The risk structures containing the autonomic nerves are shown in yellow, while the target structures are visualized in red/white (mesorectum) and red (tumor). The colors of the bone and risk zones are based on anatomical illustration standards, e.g., always coloring bone white and nerves yellow. Since the mesorectum and tumor are the target structures and this signifies importance, we use the color red to visualize these. Since there is no anatomical illustration standard for coloring the vagina and bladder, we chose colors that do not interfere with the perception of the underlying red color, and base our choices on the fact that red, green, yellow, and blue are hard-wired into the brain as primaries and should be considered first [48]. A linked 3D cursor (red sphere) relates the MRI data to the 3D model. When clicking on a structure in the 3D view, the MRI slice updates to the point corresponding to the clicked location. In the split view, the inte-

rior of the mesorectum can be explored while the cut structures can be displayed in their original form in the center on mouse hover. In the application, one of the four proposed distance confidence representations can be chosen to reveal the confidence in the outcome of the registration process, i.e., blended grid, halftone, contour confidence and contour blur. Individual structures can be made visible or invisible through selection. A surgical view is also available in which the structures are visualized from a familiar surgical orientation.

In Figure 6, two different datasets are shown based on scans of two patients. The first patient is a 71-year old female who has a mid-rectal tumor, while the second patient is a 92-year old female that has a low-rectal tumor. In comparison, the organ shapes between them vary a lot, as is typical for soft tissues such as these. Especially organs such as the bladder and rectum, which can have different levels of filling at the time of the scan, result in large size and shape variations. The tumor distance visualizations on the mesorectal wall reveal the mid- and low-rectal location of the tumor respectively. Furthermore, the unfolded view shows that in the first dataset, the tumor is located on the ventral side of the mesorectal fascia, while the second dataset tumor is located more towards the back. The color-coding and unfolded visualization show the proximity of the tumor to the mesorectal wall and the chances of a clean circumferential margin.

8 EVALUATION

In this section, we describe the setup and results of our evaluation with five domain experts and ten non-domain experts.

8.1 Evaluation Setup

We evaluated the utility of our method with five domain experts: S1, S2, S3, S4 and S5. S1 is an oncologic surgeon who is specialized in the surgical treatment of rectal cancer. He has over 20 years experience as a surgeon. S2 is a medical resident who recently obtained her PhD in surgical anatomy. She plans to be a surgical oncologist and she is one of the domain experts involved in this project. S3 is a researcher and surgical oncologist in training who finishes her training next year. In her post-doctoral research, she focuses on imaging strategies for treatment response to therapy in rectal and breast cancer. S4 is a surgical oncologist with over 12 years surgical experience. S5 is a gynecologist in training with 7 years of experience in general medicine and surgery.

After a short demonstration of the features of our application, the participants were encouraged to interact with the tool. We allowed the participants to comment or pose questions during their session and afterwards asked several open questions in a semi-structured interview. Finally, we asked the participants indicate their (dis)agreement with 30
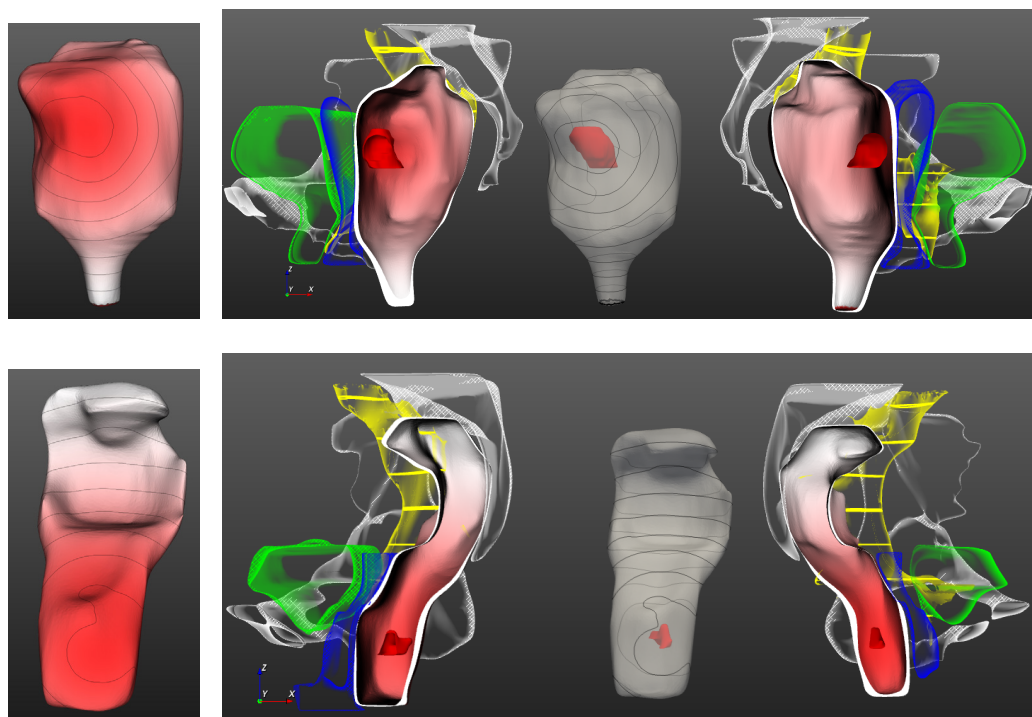
Fig. 6: Tumor distance and unfolded visualization for two datasets featuring a mid-rectal tumor and a low-rectal tumor respectively.

statements using a five-point Likert scale (see Table 1). The 30 statements were categorized into the following topics: General application (A), Context structure visualization (B), Target structure visualization (C), Risk structure visualization (D), MRI visualization (E), and Interaction (F).

In the form, the question order was randomized and symmetry was maintained by having equal numbers of positive and negative positions to prevent bias. However, for the ease of interpretation in the table, we rephrased the negative statements (indicated by a ⋆) to their positive form and inverted the scores, as described in the Sage handbook of methods in social psychology [41]. Additionally, participants were asked to rate the effectiveness of the four distance confidence visualization options in Figure 3 on a scale of 1 to 10.

To quantitatively evaluate the effectiveness of the four visual encodings of the combined distance and confidence, we performed an additional task-based evaluation with 10 non-expert participants. We presented 8 circular patches of parts of the mesorectum in the four confidence visualization styles. These patches were deemed safe or unsafe, either through their distance to the risk zones or due to high uncertainty. We asked the participants whether these regions are safe or not, and how sure they were about their answer. We measured the time that it took them to get to their answers.

8.2 Evaluation Results

During the semi-structured interview, S1 mentioned that he sees strong potential in our work for surgeons in training. Especially if we process interesting or difficult cases in several pathology categories and represent them in our tool, it can help surgeons in training to better understand the anatomy and relations between the MRI and the 3D situation. Experienced surgeons can make the translation from MRI to 3D anatomy more readily. He stated that even for experienced surgeons, sometimes the 3D reconstructions can reveal details that are not immediately apparent from the MRI, due to cognitive blind spots and selective perception. In particular, he appreciated the, to him, novel distance contour representations and interactive unfolding. While he describes the registration uncertainty and influence on the distance to the risk zones as important, he states that surgeons should always be aware that the tool provides an indication of the areas, but no exact definitions. A remaining challenge to get the tool into clinical practice, according to him, is to further automate the registration process, so that

MRI organ segmentation is no longer needed.

S2 sees potential in our work for both surgeons in training and experienced surgeons. She states that experienced surgeons can still benefit from our tool in difficult tumor cases. She especially appreciated the linked views between the MRI and the 3D representations. Her suggestions for improvement of the application are to include more anatomical structures such as the levator ani muscle and the anal sphincter complex. Both these structures are visible from the MRI and available from the atlas. Furthermore, she would find it useful if surgeons were able to store viewing preferences.

S3 especially appreciates the contours indicating the structures in the MRI view and the linked 3D cursor. She thinks this really helps surgeons in training to relate the 2D MRI data to 3D anatomy. Furthermore, the unfolded view helps her understand the relation of the tumor to the mesorectal fascia in a clearer way. She also appreciates the surgical view and viewing the MRI and the 3D model from that perspective. She indicates that an extended version of the current application could also be useful during the operation itself additionally.

S4 states that he sees a clear benefit in our application for surgical education, as well as for surgical planning. He mentions that positive resection margins are often found on the ventral part of the mesorectum, near the vaginal wall/prostate, and that it is a surgically difficult area, which can be clearly visualized with our application. He emphasizes that the annotation of the tumor in the MRI must be done by a radiologist to prevent incorrect assumptions in planning the procedure. If that condition is met, he thinks it can raise awareness of surgeons in the pre-operative planning phase and that they can transfer this knowledge into the operating theater. In the future, he would like to see the application made available for surgical guidance, by tracking and registering the position and viewpoint of surgical tools.

S5 finds the application very useful and clear. She responded positively to the visualization of the context, target and risk structures. Furthermore, she sees a clear need for this application in surgical training. She finds the representations visually pleasing.

The level of agreement of the participants with the 30 statements that were presented can be seen in Table 1. In general, all participants agree that the application is useful in pre-operative planning and has added value over the current situation (A2, A4, A5, A6). S1 stated that the application can only improve TME planning in clinical practice if the registration and segmentation is further automated, therefore, he gives a

Table 1: User response to 30 statements on a 5-point Likert-scale: 1: Strongly disagree, 2: Disagree, 3: Neither agree nor disagree, 4: Agree, 5: Strongly agree. Negatively phrased statements in the original form are indicated by a ★ and their scores are inverted for ease of interpretation.

	Statement	S1	S2	S3	S4	S5
A1	The application can improve the planning of a TME procedure	3	5	4	5	4
A2	The application can help surgeons in training in preparing a TME procedure	5	5	5	5	4
A3	The application has value in the OR during the surgery ★	3	3	2	2	2
A4	I would find this application useful in preparing a surgery ★	4	5	5	4	5
A5	The application has added value over the current situation ★	4	4	4	4	5
A6	With this application, potential surgical complications during the procedure are easier to predict	2	4	4	4	4
A7	I would like to use this application to explain the procedure to my patients	5	4	2	1	5
B1	The context organs are clearly visualized	5	5	5	5	5
B2	The context organs do not hamper the view on the important structures ★	5	4	4	5	4
B3	The context organs help me with spatial orientation	5	4	5	4	4
B4	The shape of the context organs is clearly visible ★	5	4	4	5	5
C1	The mesorectum is clearly visible at all times	5	5	4	5	4
C2	I can estimate the distance of the tumor to the mesorectal fascia well in 3D ★	4	4	5	4	5
C3	I can estimate the distance of the risk zones to the mesorectum in 3D	4	5	4	4	5
C4	The uncertainty resulting from the registration can be clearly interpreted from the visualization ★	4	4	4	4	4
C5	The contours help me estimate the distances to the mesorectum (tumor and risk)	4	3	5	5	4
C6	The color-coding (red to white) helps me estimate the distances to the mesorectum (tumor and risk)	4	4	5	4	5
D1	The risk zones that contain the autonomic nerves are clearly visible in 3D ★	4	4	4	4	5
D2	The lines in the risk zones help me estimate the height of structures	4	4	4	5	5
D3	The changes in risk zone shape at different levels are easier to interpret in 2D than 3D	4	1	1	2	2
D4	Showing the autonomic nerve zones is of added value for an experienced surgeon ★	4	5	2	2	4
D5	Showing the autonomic nerve zones is of added value for a surgeon in training	5	5	5	5	5
E1	The contours on the MRI are of added value for an experienced surgeon ★	3	4	4	2	4
E2	The contours on the MRI are of added value for a surgeon in training	4	5	5	5	5
E3	The MRI slice in the 3D visualization helps me with spatial orientation ★	4	4	5	5	5
E4	The size of the tumor is the most clearly visible in the MRI	4	2	2	4	3
F1	Unfolding the structures helps me see the interior of the mesorectum ★	4	4	4	3	4
F2	Unfolding the structures helps me to estimate the distance of the tumor to the mesorectal fascia	4	4	5	3	4
F3	The surgical view is of added value in addition to the default view ★	5	4	5	5	3
F4	The 3D cursor (red sphere) helps me connect the 3D and 2D visualizations	5	5	4	5	5

Table 2: Confidence visualization option ratings.

Representation	S1	S2	S3	S4	S5
Blended gridlines	7.00	7.00	7.00	6.00	8.00
Halftone	7.75	8.00	8.00	7.00	10.00
Isoline confidence	7.00	3.00	6.00	9.00	10.00
Isoline blur	8.25	7.00	5.00	8.00	8.00

Representation	Accuracy	Avg time	Confidence
Blended gridlines	0.80	10.17	3.01
Halftone	0.85	9.99	2.90
Isoline confidence	.95	10.73	2.79
Isoline blur	0.75	10.00	2.57

relatively low score in A2. All users agree that the application is not yet ready to be brought into the OR at this point (A3), however, they see the potential for an extension of this work. Some surgeons would like to use the application to explain the procedure to the patients, while others think the patients already get overwhelmed by too much information and it would take too much time to explain what the application shows (A7).

The visualization of the context and target organs was positively to very positively evaluated by all participants (B1 to C6). Especially the visualization of context organs was found to be very clear by all. While the risk zone indication was found to be clear (D1, D2), not all participants agreed it would be useful to experienced surgeons, indicating they expect this information is already known to them (D4). Interestingly enough, the most experienced surgeons, S1 and S4, did evaluate this positively, even for experienced surgeons such as themselves. For surgeons in training, all participants strongly agreed that it would be useful to show these zones (D5). While S1 preferred the 2D MRI view to see the risk zone shape varying per level, all others preferred the 3D visualization (D3).

The MRI visualization was found useful in both 2D and 3D and useful especially to surgeons in training, though S4 pointed out that experienced surgeons will already be able to interpret this information (E1, E2, E3). While two of the participants preferred to estimate the size of the tumor in the MRI, two preferred the 3D view for this purpose (E4). The unfolding interaction to reveal the relation between the tumor and the mesorectal fascia was rated positively by all surgeons (F1, F2). The surgical view was found beneficial by four out of five participants (F3). The 3D linked cursor between the MRI and 3D representation was found very helpful by all participants.

In the top of Table 2, we present the responses of the expert participants regarding the visual encoding options to visualize the confidence of the risk zone distance on the mesorectum. In general, the response to all visual encodings was positive, but each participant had a personal preference towards one or two of the encodings. The option that was ranked the highest on average by the users is the halftone representation, while no participant had a real preference for the blended grid approach. All participants appreciate the clarity and intuitive understanding the halftone representation brings. The other representations were met with mixed responses. Especially the isoline confidence representation generated polarizing responses. While some participants thought it was very clear, others were confused by the view.

In the bottom of Table 2, we present the conclusions of the task performance experiment with ten non-experts. The accuracy (number of correct answers divided by the total number of tasks) was highest for the isoline confidence, and worst for the isoline blur, but only by a small difference. Average times were also similar. The participants felt more confident in their answers with the global methods, but again by a small amount.

8.3 Evaluation Conclusion

From Table 1, we conclude that the application was rated positively overall. Every participant saw the benefits of our application in im-

proving surgical planning for surgeons in training. Furthermore, the surgeons indicated that for difficult cases, the application is also of value to experienced surgeons. The visualization of the context and target structures was found to be clear in both the enriched 2D MRI representation and the 3D models. While opinions varied on the utility of showing the risk zones to experienced surgeons, the visual representation was again found to be clear in both 2D and 3D. The MRI visualization and relation to the 3D anatomy was found to be a valuable addition. Furthermore, the interaction options helped the surgeons get insight into this relation, as well as the relation between the tumor and the mesorectal fascia. Among the confidence visualization options, the halftone representation was found to be the most effective by the experts on average. In the quantitative evaluation of these four combined distance and confidence representations, there was no clearly better or worse performing representation, indicating that either a more thorough user study is needed with more data and participants, or that the choice of representation is mainly a personal preference.

9 DISCUSSION

In the analysis of this problem domain, we found several distinguishing features that set this particular application apart from other surgical-planning visualization applications. Especially the combination of complex anatomy and visualizing structures, which are invisible during surgery or in the scans, provides a challenge that distinguishes surgical planning for pelvic oncological procedures from surgical planning in other domains. While surgical planning visualization systems often focus on access planning, implant planning or reconstruction planning, in our case improving the spatial understanding of anatomy and pathology is the main focus. In the TME procedure specifically, due to the confined space and the fact that the complete mesorectum needs to be excised, the surgical planning phase is not about planning an access path, but more about choosing the type of surgery that is most appropriate for the pathology. Furthermore, the surgeon needs to be aware of the location of the autonomic risk zones surrounding the mesorectum in order to prevent damaging them. Since the zones in which the autonomic nerves reside in our atlas are defined quite coarsely, it is questionable if this information brings much new knowledge to experienced surgeons, who are already aware of these regions, but would like to see the exact spatial extent.

This particular problem domain poses several general visualization challenges. The complex pelvic anatomy, featuring many closely arranged structures that vary quite extensively in shape and size between patients, results in the need to illustrate the spatial anatomical context without distracting or occluding the structure that needs to be resected. For this, illustrative visualization methods with a high level of abstraction are especially suitable. Furthermore, the 'invisible' regions containing the risk structures and the distance of these regions to the target structure need to be emphasized without occluding the target structure. Finally, the confidence in the outcome of the registration process and the influence on these distances needs to be visualized in order to not mislead the user with a false sense of accuracy. Since this confidence is related to the distance, both information types need to be conveyed in visual channels that can be perceived simultaneously.

The limitations of our approach lie mainly in the atlas itself, the registration process and the amount of time required for the preprocessing steps. Our method relies on the risk zones defined by the atlas, which has limited accuracy, e.g., it does not include multiple individuals and it exclusively contains female pelvic anatomy. The atlas deals with anatomical variability by defining the risk zones in a broad region to account for all possible individual variations. Further improvements in the atlas and a more specific definition of the risk zones via cadaveric studies would have beneficial consequences for our application.

The registration confidence calculation could be improved to reveal more information about the uncertainty, by including for instance in which direction the mismatch occurred. This could provide more insight into the influence of the registration confidence on the risk zone distance calculation.

Currently there is pre-processing required in terms of segmentation, registration and distance calculation. While the distance calculation

and registration processes themselves are fast, the manual segmentation of the MRI scan still takes up to 30 minutes. To bring our method into clinical practice for pre-operative planning purposes, this time needs to be reduced. We could achieve this by further automating the segmentation process. Once many MRI scans are registered to the atlas, we can perform MRI to MRI registration and employ atlas-based segmentation to automatically segment the major organs and bone structures from the MRI scan. Atlas-based segmentation is already successfully applied to brain and cardiac segmentation tasks [5].

Despite these limitations, as shown in the evaluation, we have provided a method that is already suitable for surgical planning, for surgeons in training and experienced surgeons alike, that forms a solid basis for further developments to bring it into clinical practice.

10 CONCLUSION AND FUTURE WORK

We presented PelVis, a method to visualize context, target and risk structures for preoperative planning of pelvic oncologic surgical procedures. Using occlusion-management and distance-based visualization techniques, the surgically relevant structures are visualized based on a patient-specific 3D model of the pelvis, acquired through atlas registration to pre-operative MRI scans. In an interactive application featuring several linked views, the spatial relations in the complex anatomy can be freely explored. From our evaluation we concluded that our prototype application has great potential in surgical planning and especially in surgical training for oncologic surgeons in training. However, before it is ready for clinical use in planning and surgical guidance, several steps still need to be taken. First, the user interface should be improved to fit the clinical requirements, e.g., minimum interaction required to get the desired information. Furthermore, the registration process should be improved so that it no longer requires manual MRI segmentation. Once we register more MRI scans to the atlas, we can create multiple atlas sets and employ atlas fusion or voting techniques to reduce preprocessing effort. We would also like to look into applying our methods to other procedures, since the methods are generally applicable and may be of value for instance in radiotherapy planning or even surgical simulation. Furthermore, this work could be extended to bring the application into the operating room and using instrument tracking to interactively update the views for surgical guidance.

REFERENCES

[1] S. Atallah, B. Martin-Perez, M. Albert, G. Nassif, L. Hunter, S. Larach, et al. Transanal minimally invasive surgery for total mesorectal excision (TAMIS–TME): results and experience with the first 20 patients undergoing curative-intent rectal cancer surgery at a single institution. *Techniques in coloproctology*, 18(5):473–480, 2014.

[2] A. Baer, R. Gasteiger, D. Cunningham, and B. Preim. Perceptual evaluation of ghosted view techniques for the exploration of vascular structures and embedded flow. 30(3):811–820, 2011.

[3] C. P. Botha and F. H. Post. Hybrid scheduling in the DeVIDE dataflow visualisation environment. In *SimVis*, pages 309–322, 2008.

[4] G. Brown, A. Kirkham, G. T. Williams, M. Bourne, A. G. Radcliffe, J. Sayman, R. Newell, C. Sinnatamby, and R. J. Heald. High-resolution MRI of the anatomy important in total mesorectal excision of the rectum. *American Journal of Roentgenology*, 182(2):431–439, 2004.

[5] M. B. Cuadra, V. Duay, and J.-P. Thiran. Atlas-based segmentation. In *Handbook of Biomedical Imaging*, pages 221–244. Springer, 2015.

[6] P.-E. Danielsson. Euclidean distance mapping. *Computer Graphics and image processing*, 14(3):227–248, 1980.

[7] C. Dick, R. Burgkart, and R. Westermann. Distance visualization for interactive 3D implant planning. *Visualization and Computer Graphics, IEEE Transactions on*, 17(12):2173–2182, 2011.

[8] S. Djurcilov, K. Kim, P. Lermusiaux, and A. Pang. Visualizing scalar volumetric data with uncertainty. *Computers & Graphics*, 26(2):239–248, 2002.

[9] J. Ferlay, E. Steliarova-Foucher, J. Lortet-Tieulent, S. Rosso, J. Coebergh, H. Comber, D. Forman, and F. Bray. Cancer incidence and mortality patterns in Europe: estimates for 40 countries in 2012. *European journal of cancer*, 49(6):1374–1403, 2013.

[10] R. Gasteiger, M. Neugebauer, C. Kubisch, and B. Preim. Adapted surface visualization of cerebral aneurysms with embedded blood flow information. In *VCBM*, pages 25–32, 2010.

[11] P. A. Georgiou, P. P. Tekkis, V. A. Constantinides, U. Patel, R. D. Goldin, A. W. Darzi, R. J. Nicholls, and G. Brown. Diagnostic accuracy and value of magnetic resonance imaging (MRI) in planning exenterative pelvic surgery for advanced colorectal cancer. *European Journal of Cancer*, 49(1):72–81, 2013.

[12] B. Gooch, P.-P. J. Sloan, A. Gooch, P. Shirley, and R. Riesenfeld. Interactive technical illustration. In *Proceedings of the 1999 symposium on Interactive 3D graphics*, pages 31–38. ACM, 1999.

[13] G. Grigoryan and P. Rheingans. Probabilistic surfaces: Point based primitives to show surface uncertainty. In *Proceedings of the conference on Visualization'02*, pages 147–154. IEEE Computer Society, 2002.

[14] C. Hansen, S. Zidowitz, M. Hindennach, A. Schenk, H. Hahn, and H.-O. Peitgen. Interactive determination of robust safety margins for oncologic liver surgery. *International journal of computer assisted radiology and surgery*, 4(5):469–474, 2009.

[15] R. Heald, E. Husband, and R. Ryall. The mesorectum in rectal cancer surgerythe clue to pelvic recurrence? *British Journal of Surgery*, 69(10):613–616, 1982.

[16] R. Heald and R. Ryall. Recurrence and survival after total mesorectal excision for rectal cancer. *The Lancet*, 327(8496):1479–1482, 1986.

[17] D. House and C. Ware. A method for the perceptual optimization of complex visualizations. In *Proceedings of the Working Conference on Advanced Visual Interfaces*, pages 148–155. ACM, 2002.

[18] V. Interrante, H. Fuchs, and S. M. Pizer. Conveying the 3d shape of smoothly curving transparent surfaces via texture. *IEEE Transactions on visualization and computer graphics*, 3(2):98–117, 1997.

[19] Y. Kinugasa, G. Murakami, D. Suzuki, and K. Sugihara. Histological identification of fascial structures posterolateral to the rectum. *British journal of surgery*, 94(5):620–626, 2007.

[20] S. Klein, J. P. Pluim, M. Staring, and M. A. Viergever. Adaptive stochastic gradient descent optimisation for image registration. *International journal of computer vision*, 81(3):227–239, 2009.

[21] S. Klein, M. Staring, K. Murphy, M. A. Viergever, and J. P. Pluim. Elastix: a toolbox for intensity-based medical image registration. *Medical Imaging, IEEE Transactions on*, 29(1):196–205, 2010.

[22] A. Krüger, C. Tietjen, J. Hintze, B. Preim, I. Hertel, and G. Strauß. Interactive visualization for neck-dissection planning. In *EuroVis*, volume 5, pages 295–302, 2005.

[23] J. Kybic. Bootstrap resampling for image registration uncertainty estimation without ground truth. *Image Processing, IEEE Transactions on*, 19(1):64–73, 2010.

[24] M. Lange, C. Marijnen, C. Maas, H. Putter, H. Rutten, A. Stiggelbout, E. M.-K. Kranenbarg, C. van de Velde, C. C. I. of the Dutch, et al. Risk factors for sexual dysfunction after rectal cancer treatment. *European Journal of Cancer*, 45(9):1578–1588, 2009.

[25] K. Lawonn, S. Glaßer, A. Vilanova, B. Preim, and T. Isenberg. Occlusion-free blood flow animation with wall thickness visualization. *Visualization and Computer Graphics, IEEE Transactions on*, 22(1):728–737, 2016.

[26] J. Leroy, F. Jamali, L. Forbes, M. Smith, F. Rubino, D. Mutter, and J. Marescaux. Laparoscopic total mesorectal excision (TME) for rectal cancer surgery: long-term outcomes. *Surgical Endoscopy and Other Interventional Techniques*, 18(2):281–289, 2004.

[27] G. E. Marai, D. H. Laidlaw, Ç. Demiralp, S. Andrews, C. M. Grimm, and J. J. Crisco. Estimating joint contact areas and ligament lengths from bone kinematics and surfaces. *Biomedical Engineering, IEEE Transactions on*, 51(5):790–799, 2004.

[28] D. F. Marshall, H. J. Gardner, and B. H. Thomas. Interactive visualisation for surface proximity monitoring. In *Proceedings of the 16th Australasian User Interface Conference (AUIC 2015)*, volume 27, page 30, 2015.

[29] M. J. McGuffin, L. Tancau, and R. Balakrishnan. Using deformations for browsing volumetric data. In *Visualization, 2003. VIS 2003. IEEE*, pages 401–408. IEEE, 2003.

[30] I. D. Nagtegaal and P. Quirke. What is the role for the circumferential margin in the modern treatment of rectal cancer? *Journal of Clinical Oncology*, 26(2):303–312, 2008.

[31] I. D. Nagtegaal, C. J. van de Velde, E. van der Worp, E. Kapiteijn, P. Quirke,

[32] J. S. Park, M. S. Chung, S. B. Hwang, Y. S. Lee, D.-H. Har, and H. S. Park. Visible Korean human: improved serially sectioned images of the entire body. *Medical Imaging, IEEE Transactions on*, 24(3):352–360, 2005.

[33] J. S. Park, M. S. Chung, S. B. Hwang, B.-S. Shin, and H. S. Park. Visible Korean human: its techniques and applications. *Clinical Anatomy*, 19(3):216–224, 2006.

[34] J. S. Park, J. W. Huh, Y. A. Park, Y. B. Cho, S. H. Yun, H. C. Kim, W. Y. Lee, and H.-K. Chun. A circumferential resection margin of 1 mm is a negative prognostic factor in rectal cancer patients with and without neoadjuvant chemoradiotherapy. *Diseases of the Colon & Rectum*, 57(8):933–940, 2014.

[35] J. S. Park, Y.-W. Jung, J. W. Lee, D. S. Shin, M. S. Chung, M. Riemer, and H. Handels. Generating useful images for medical applications from the visible Korean human. *Computer methods and programs in biomedicine*, 92(3):257–266, 2008.

[36] A. Pigazzi, J. Ellenhorn, G. Ballantyne, and I. Paz. Robotic-assisted laparoscopic low anterior resection with total mesorectal excision for rectal cancer. *Surgical Endoscopy and Other Interventional Techniques*, 20(10):1521–1525, 2006.

[37] B. Preim and C. P. Botha. *Visual Computing for Medicine: Theory, Algorithms, and Applications*. Newnes, 2013.

[38] P. J. Rhodes, R. S. Laramee, R. D. Bergeron, T. M. Sparr, et al. Uncertainty visualization methods in isosurface rendering. In *Eurographics*, volume 2003, pages 83–88, 2003.

[39] C. Rieder, T. Kroeger, C. Schumann, and H. K. Hahn. GPU-based real-time approximation of the ablation zone for radiofrequency ablation. *Visualization and Computer Graphics, IEEE Transactions on*, 17(12):1812–1821, 2011.

[40] D. Rueckert, L. I. Sonoda, C. Hayes, D. L. Hill, M. O. Leach, and D. J. Hawkes. Nonrigid registration using free-form deformations: application to breast MR images. *Medical Imaging, IEEE Transactions on*, 18(8):712–721, 1999.

[41] C. Sansone, C. C. Morf, and A. T. Panter. *The Sage handbook of methods in social psychology*. Sage Publications, 2003.

[42] N. N. Smit, B. K. Haneveld, M. Staring, E. Eisemann, C. P. Botha, and A. Vilanova. Registrationshop: An interactive 3D medical volume registration system. In *VCBM*, pages 145–153, 2014.

[43] J. Süßmuth, W.-D. Protogerakis, A. Piazza, F. Enders, R. Naraghi, G. Greiner, and P. Hastreiter. Color-encoded distance visualization of cranial nerve-vessel contacts. *International journal of computer assisted radiology and surgery*, 5(6):647–654, 2010.

[44] M. Termeer, J. O. Bescós, M. Breeuwer, A. Vilanova, F. Gerritsen, M. E. Groller, and E. Nagel. Visualization of myocardial perfusion derived from coronary anatomy. *Visualization and Computer Graphics, IEEE Transactions on*, 14(6):1595–1602, 2008.

[45] A. F. van Dixhoorn, J. Milles, B. van Lew, and C. P. Botha. BrainCove: A tool for voxel-wise fMRI brain connectivity visualization. In *VCBM*, pages 99–106, 2012.

[46] I. Viola and E. Gröller. Smart visibility in visualization. In *Computational Aesthetics*, pages 209–216, 2005.

[47] C. Wallner, M. M. Lange, B. A. Bonsing, C. P. Maas, C. N. Wallace, N. F. Dabhoiwala, H. J. Rutten, W. H. Lamers, M. C. DeRuiter, and C. J. van de Velde. Causes of fecal and urinary incontinence after total mesorectal excision for rectal cancer based on cadaveric surgery: a study from the Cooperative Clinical Investigators of the Dutch total mesorectal excision trial. *Journal of clinical oncology*, 26(27):4466–4472, 2008.

[48] C. Ware. *Information visualization: perception for design*. Elsevier, 2012.

[49] R. T. Whitaker, M. Mirzargar, and R. M. Kirby. Contour boxplots: A method for characterizing uncertainty in feature sets from simulation ensembles. *Visualization and Computer Graphics, IEEE Transactions on*, 19(12):2713–2722, 2013.

[50] A. Wibe, P. Rendedal, E. Svensson, J. Norstein, T. Eide, H. Myrvold, and O. Søreide. Prognostic significance of the circumferential resection margin following total mesorectal excision for rectal cancer. *British Journal of Surgery*, 89(3):327–334, 2002.

[51] I. Wolf, M. Vetter, I. Wegner, T. Böttger, M. Nolden, M. Schöbinger, M. Hastenteufel, T. Kunert, and H.-P. Meinzer. The medical imaging interaction toolkit. *Medical image analysis*, 9(6):594–604, 2005.

J. H. J. van Krieken, et al. Macroscopic evaluation of rectal cancer resection specimen: clinical significance of the pathologist in quality control. *Journal of Clinical Oncology*, 20(7):1729–1734, 2002.